Residual Stress Determination of Silicon Containing Boron Dopants in CMCs[1,2]

Michael W. Knauf*[3], Craig P. Przybyla**, Andrew J. Ritchey***, Rodney W. Trice****, R. Byron Pipes*****
* School of Aeronautics and Astronautics, Purdue University, West Lafayette, IN, 47907
** Air Force Research Laboratory, Wright-Patterson Air Force Base, OH, 45435
*** Rolls-Royce Corporation, Indianapolis, IN, 46225
**** School of Materials Engineering, Purdue University, West Lafayette, IN, 47907
***** Schools of Aeronautics and Astronautics, Materials Engineering and Chemical Engineering, Purdue University, West Lafayette, IN, 47907

Abstract

Raman spectroscopy was utilized to investigate residual stresses found within a SiC/SiC ceramic matrix composite containing Hi-Nicalon™ fibers, a slurry melt-infiltrated matrix of silicon carbide particles, and silicon matrix. Large gradients of electrically-active boron are found throughout various regions within the crystalline lattice of the silicon matrix. The regions were identified by the varying degrees of asymmetry and peak width measured in the resonant Fano profile of the doped silicon. A methodology to determine the residual stress state of silicon exhibiting varying degrees of electrically-active boron is presented by utilizing the changes in the Raman profile parameters. Previous works on similar SiC/SiC CMCs have attributed spatial gradients in the wavenumber to large fluctuations in stress. By applying the proposed methodology, we show that these observations are related to active boron that is segregated in various matrix areas. Utilizing this methodology, mean compressive stresses in various silicon regions were found to be approximately 300 MPa, with complementary tensile silicon carbide particle stresses of approximately 300 MPa.

---

[1] Based upon Knauf dissertation entitled "Effects of Heat Treatment on SiC-SiC Ceramic Matrix Composites," Purdue University, 2017. Partially presented at 2018 United States Advanced Ceramics Association conference, Cape Canaveral, FL.

[2] Research funding provided by US Air Force, materials provided by Rolls Royce.

[3] Active-duty Air Force officer, currently stationed at Arnold Air Force Base, TN, 37389. E-mail: Michael.Knauf@us.af.mil

1.0 Introduction

Ceramic Matrix Composite (CMC) materials are poised to replace many traditionally metallic high-performance alloy components in hot sections of jet turbine engines, greatly increasing efficiency and available thrust[1, 2]. There are inherent difficulties in producing these materials, not least of which is controlling the levels of residual stress within the composite. The stresses come as a result of coefficient of thermal expansion mismatch between constituents, intrinsic stresses developed during chemical vapor infiltration[3], and possibly crystallization expansion of silicon resulting from a significant volume increase in the phase transition from liquid to solid[4]. To capitalize on the vast benefits of CMCs, the full residual stress state must be understood, predicted, and controlled. Various authors have experimentally determined residual stress states through Raman spectroscopy[4, 5], X-ray diffraction[6, 7, 8], and the common intersection point method[9, 10]. The reported stresses determined through these multiple techniques vary by orders of magnitude. Of the various methods available to study residual stresses, Raman spectroscopy requires relatively little material and provides spatial resolutions of $1\ \mu m$ or less, making it an invaluable tool in stress determination at the microscopic level[11].

Anastassakis[12, 13] developed a methodology to determine the stress in a silicon crystal by linearly correlating the level of strain within the material to the change in the Raman characteristic wavenumber, $\Delta\omega$ (normally the peak center of a Lorentzian profile). Assuming the strain is lower than the elastic limit, this can then be correlated to the stress found within the constituents. Typically, the relationship between stress and change in wavenumber is reported directly. For many materials, this shift linearly corresponds to a change in the hydrostatic stress state of the constituent

being interrogated. Depending on the known loading, this hydrostatic stress (σ_H) can be correlated to stress in distinct directions (e.g. uniaxial, biaxial, or hydrostatic)[14]. This methodology can also be applied to many crystalline materials, including CMC constituents such as polycrystalline silicon, silicon carbide and Hi-Nicalon™ fibers (Nippon Carbon Co., Ltd, Tokyo, Japan)[13, 15, 16].

Pure silicon exhibits a linear shift in peak location with applied stress for the peak nominally located at $520.5\ cm^{-1}$. This peak is triply degenerate, and remains degenerate with applied stress under normal circumstances. Therefore, only the hydrostatic component of the stress tensor ($\Delta\sigma_H$) can reliably be ascertained through Raman spectroscopy. When stressed, the wavenumber shifts according to Equation 1:

$$\Delta\sigma_H = \Delta\omega \times C \qquad \text{Equation 1}$$

Where $C_{Si} = -0.177\ GPa/cm^{-1}$ for silicon[14]. The 6H polytype of silicon carbide exhibits an analogous wavenumber shift of $C_{SiC} = -0.283\ GPa/cm^{-1}$ for the primary peak at $789\ cm^{-1}$ with applied stress[15].

Raman spectroscopy is considered a surface technique as most materials readily absorb and/or reflect the incident laser light within a few micrometers or less[17]. An absorption depth, δ, can be defined to compare the relative depths of penetration of a particular laser wavelength in different materials as $\delta = 1/\alpha$, where α is the absorption coefficient for the material. This is the depth at which the intensity of the incident light decreases by 63% $(1 - 1/e = 63\%)$[18]. Linear interpolation of silicon absorption coefficient values determined by Aspnes and Studna[19] for a green $514.5\ nm$ wavelength laser (such a laser was utilized in subsequent investigations) provides an absorption

coefficient of approximately $15000\,cm^{-1}$. Taking the reciprocal gives the effective depth of penetration of approximately $0.67\,\mu m$ for this laser. Therefore, silicon measurements utilizing Raman spectroscopy are effectively a surface technique.

Silicon carbide, however, is relatively transparent to green $514.5\,nm$ laser light. Linear interpolation of absorption coefficient data given by Derst et al.[20] for crystalline SiC provides an absorption coefficient of approximately $14\,cm^{-1}$. The corresponding penetration depth is $710\,\mu m$. This result has two repercussions; first, the stress measured by Raman spectroscopy in SiC has a volumetric element and should not be modeled as a plane stress state (a common assumption in surface measurements). Second, it is possible to capture the Raman signature of the silicon matrix below any SiC particulates, and the stress state of this silicon will be three-dimensional as well.

Boron is a common additive (dopant) in silicon melt-infiltrated composites[21], and has a major influence on many of the processes involved in residual stress measurement. Silicon dopants in groups IIIA and VA of the periodic table (including boron) introduce an asymmetric profile shape in the Raman signature, termed Fano resonance[22, 23, 24]. This is due to the Fermi level (chemical potential of electrons) moving out of the semiconductor band gap and towards either the conduction band or the valence band of silicon, depending on the dopant used. Thus, these silicon dopants change the electronic structure of silicon and affect the Raman signature, estimated by a Fano line shape[24, 25, 26]. The effects of the Fano resonance must be removed prior to stress determination to accurately measure the stress in silicon which contains group IIIA or VA elements. Fano resonance affects the silicon profile in several ways: 1) it introduces asymmetry to a normally symmetric Raman spectra; 2) the silicon peak center is shifted away from the normal stress-free silicon value of 520.5 cm^{-1}; 3) it shifts the characteristic wave number even further from the stress free value so that it no longer

corresponds to the peak center as is the case for symmetric profiles; and 4) it increases the width of the spectra. Agaiby et al.[27] utilized the asymmetry of the Fano profile to estimate the dopant concentration, and thus separate the wavenumber shift contributions of the boron dopant and stress state. The method employed by Agaiby et al. was over a narrow range of dopant concentrations (up to $5 \times 10^{19}\ atoms/cm^3$) and limited laser wavelengths (488 nm, 514 nm, and 633 nm). Chandrasekhar[24] noted the Fano profile asymmetry parameter is inconsistent between different laser wavelengths. Therefore, as an alternative, the spectra width can be used, which is relatively consistent between laser wavelengths, and literature provides much larger dopant concentration ranges for the stress-free wavenumber shift contributions[24].

In the current work, the residual stress state of a slurry melt-infiltrated ceramic matrix composite is studied using Raman spectroscopy. The material system is a Rolls-Royce composite produced with Hi-Nicalon™ fibers woven into a five-harness satin weave, coated with boron nitride and silicon carbide, and subsequently infiltrated with silicon carbide particles and a boron-doped silicon matrix. The Fano effects on the silicon Raman signature caused by boron doping are separated from the Raman shift measured in the silicon phase induced by residual stress, thus providing accurate residual stress measurements for the silicon and silicon carbide constituents.

2.0 Experimental Procedure

2.1 Sample Preparation

Residual stress measurements were made on specimens cut from a $4\ mm$ thick SiC/SiC slurry melt-infiltrated CMC plate. A surface grinder equipped with a diamond blade made initial cuts from

the host plate, plunging at increments of $1\ \mu m$ per pass with a water-based lubricant. Sectioning to various smaller sizes was performed using a low speed diamond cutoff saw (VC-50, LECO Corp., St. Joseph, MI). One specimen was sectioned to $25\ mm \times 25\ mm \times 4\ mm$, while another was sectioned to $4\ mm \times 3\ mm \times 4\ mm$. The smaller sample size was required to investigate the viability of Raman spectroscopy for follow-on experiments in a high temperature heated stage which utilizes a small crucible. The Raman results for this small sample were compared to the results of the larger sample to validate that significant residual stresses were not released when machining the relatively small sample. All samples were polished using successive diamond polishing compounds of $6\ \mu m$, 3 μm, and 1 μm.

Stress-free reference samples were needed for the silicon as the published stress-free wavenumbers for pure silicon are invalid when Fano resonance is present (detailed in Discussion below). As part of the manufacturing process, the surface of the as-manufactured CMC plates had small globules of highly-doped silicon that extend 1 mm or more past the bulk of the plate surface. The apex of these globules were assumed to be stress-free because they are relatively far from the fibers and other constituents which would produce residual stresses from CTE mismatch and silicon expansion upon freezing. Four suitable globules were polished using successive diamond polishing compounds of $6\ \mu m$, 3 μm, and 1 μm and investigated with Raman spectroscopy.

2.2 Raman Spectroscopy Measurement Procedure

The $514.5\ nm$ line of an Ar+ laser (Stellar-REN, Stellar Pro, Centerville, Utah) was used with a Raman system (Renishaw inVia, Renishaw PLC, Wotton-under-Edge, United Kingdom) incorporating a backscattering arrangement. The Raman microscope was equipped with a grating of

$1800\ lines/mm$, providing the required range to study both silicon and silicon carbide signatures in the same measurement. The laser power was kept to less than $2\ mW$ at the sample to prevent heating issues from the laser while providing strong signal. Two accumulations, each 10 seconds long, were taken of each point. A laser spot size of approximately $1\ \mu m$ was produced with a 100x objective. The Raman shift of a single silicon crystal standard reference was used to calibrate the equipment.

Three areas of silicon were observed using the Raman system: underneath silicon carbide particles (which also produced a silicon carbide spectra because SiC is opaque to $514.5\ nm$ light), on the surface of the matrix, and within the fiber tow. At least sixty point measurements were taken of each area, including data from both the large and small as-received samples. Examples of the SiC particles and surface matrix microstructure are found in Figure 1, where the dark SiC particles are seen within a light-colored silicon matrix. Figure 2 illustrates the coated Hi-Nicalon™ fibers with a centrally-located silicon section. All measurements were randomly chosen throughout the central area of each specimen, and were centered in each feature as shown where the "X" marks a common example laser location. Finally, an intratow area (shown in Figure 3) was mapped in $1\ \mu m$ steps utilizing the same Raman equipment.

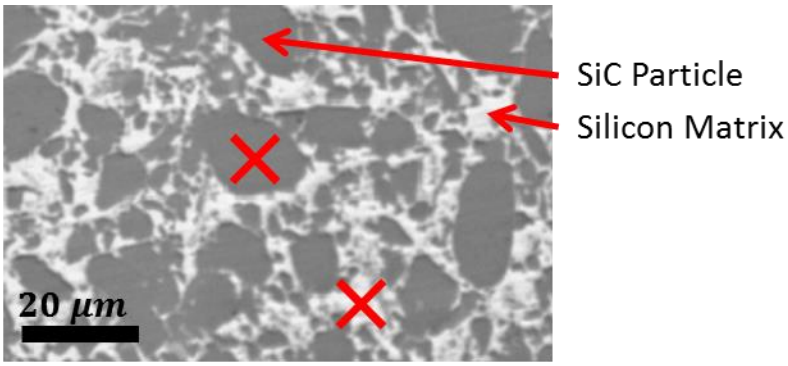

Figure 1: The dark gray particles are silicon carbide, while the light gray matrix is doped silicon. Example common Raman measurement locations are identified by X's: A) SiC particle/silicon below SiC particle, and B) surface silicon.

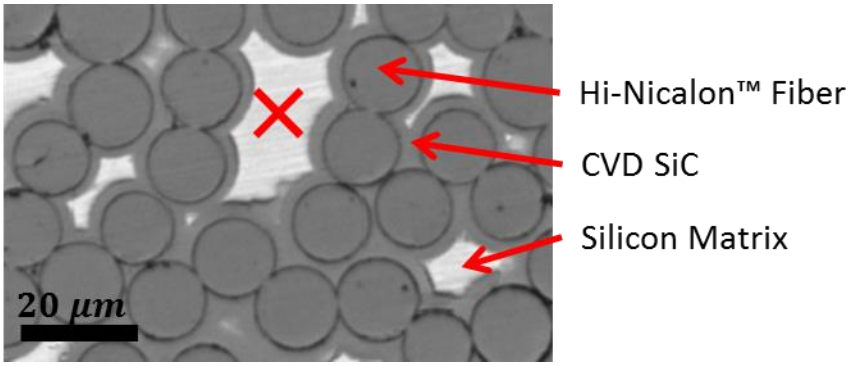

Figure 2: The dark gray circles are Hi-Nicalon™ fibers with a very dark overcoat of boron nitride, and an additional overcoat of silicon carbide. The veins are filled with doped silicon (light gray) during the melt infiltration step.

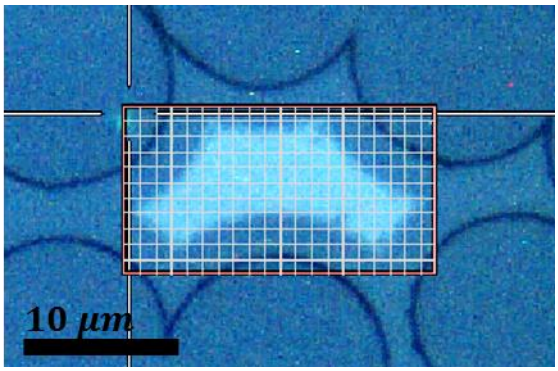

Figure 3: A Raman measurement map was investigated of an intratow area. Measurements were taken at each grid intersection, corresponding to 1 μm increments. Results of this mapping show large gradients in the activated boron concentration within the intratow silicon.

2.3 Residual Stress Determination

The Raman signatures of pure silicon and silicon carbide are represented by Lorentzian distributions[11, 12, 13, 15], described by Equation 2,

$$I(\omega)_{\mathrm{i,Lorentz}} = \frac{I_0}{\Gamma\left(1 + 4\left(\frac{\omega - \omega_0}{\Gamma}\right)^2\right)} \qquad \text{Equation 2}$$

where $I(\omega)$ is the functional value of the equation, I_0 is an arbitrary pre-multiplier, Γ is the full width of the peak at half of the maximum peak height (FWHM), ω_0 is the peak center, and ω is the abscissa.

The Fano line shape found in doped silicon can be described by Equation 3,

$$\mathrm{I}(\omega)_{\mathrm{i,Fano}} = \frac{\mathrm{I}_0\left(q + \left(\frac{\omega - \omega_0}{\Gamma}\right)\right)^2}{1 + \left(\frac{\omega - \omega_0}{\Gamma}\right)^2} \qquad \text{Equation 3}$$

where ω is the abscissa, q is the asymmetry parameter, ω_0 is the Fano wavenumber, Γ is the half width at half of the maximum peak height (as opposed to the full width at half of the maximum peak height used in the Lorentz equation), and I_0 is an arbitrary fitting constant. The peak position is offset from the characteristic wavenumber, ω_0, to $\omega_0 + \Gamma/2q$. The Fano line shape approaches a Lorentzian in the limit of $q \to \infty$. The data points produced through Raman microscopy can be fitted with a summation of Lorentzian and Fano line shapes, along with a linear baseline, to determine the characteristic wavenumbers of the various peaks, as shown in Equation 4.

$$I_{total}(\omega) = \sum_{i=1}^{n} I(\omega)_i + \mathrm{A}(\omega) \qquad \text{Equation 4}$$

A curve represented by $I(\omega)_i$ is added for every peak (Lorentz or Fano) present in the spectra, $A(\omega)$ is the linear baseline, $I_{total}(\omega)$ is the overall functional value at the various data points, and ω is the abscissa. In this work, the curve is fit using a non-linear least squares MATLAB routine. By fitting the whole profile at once, resulting parameters found through the fitting routine represent very accurate peak measurements (approximately $\pm 0.1\ cm^{-1}$[17]).

3.0 Results and Discussion

3.1 Dopant Activation and Stress Measurement

For any dopant to affect the electronic characteristics of silicon, it must be electrically-active. For boron, activation requires individual boron atoms to be covalently bonded to four silicon atoms as a substitutional atom in the overall silicon tetrahedral crystal lattice arrangement. This activation significantly reduces the resistivity of a silicon semiconductor, and is thus of interest to the semiconductor industry[28]. Full activation is difficult to achieve. Precipitation of silicon borides in silicon causes electrical inactivity of boron due to boron atoms being absorbed by SiB_x structures[29]. Alternatively, boron can form interstitial clusters which can render many boron atoms inactive within silicon[26]. These clusters have the ability to dissolve at temperatures greater than 850°C[30]. Additionally, the manufacturing environment can also lead to boron deactivation, as in the case of hydrogen saturating one of the four tetrahedral silicon bonds[28]. Finally, compressive strains at high temperatures have also been found to increase the amount of substitutional boron within the silicon lattice, while tensile strains decrease the amount of boron dissolved[26, 31].

Chandrasekhar et al.[24] determined that a Fano-type Raman spectroscopy resonance profile replaces the normally Lorentzian profile of silicon at $520.5\ cm^{-1}$ for boron-doped silicon. This is

due to the Fermi level entering the valence band of highly p-doped silicon at boron concentrations greater than approximately $10^{19}\ atoms/cm^3$ at room temperature, producing a degenerate semiconductor. Localized vibrational modes also appear as Fano line shapes at $\sim 620 cm^{-1}$ and $\sim 644 cm^{-1}$ as a result of doping. The former is attributed to the ^{11}B isotope, while the latter is attributed to the ^{10}B isotope. The intensities of the two peaks follow that of boron's natural isotope occurrence, namely 80% is found as ^{11}B and 20% is found as ^{10}B. In the same study, Chandrasekhar also determined that the width and asymmetry of the primary Fano profile is dependent upon the dopant concentration. The asymmetry is additionally dependent on the laser wavelength used, while the width is relatively constant between different wavelengths. The proposed technique utilizes this information to determine the stress free wave number as a function of peak half width to correct for boron concentration. These values are summarized for a $514.5\ nm$ laser in

Table 1. Asymmetry parameters are missing in the table because they are dependent on the wavelength of the laser.

This work primarily uses the stress-free Fano parameter values from the work of Chandrasekhar et al.; however, the dopant concentrations found in the CMC under investigation are greater than the maximum concentrations found in literature. Therefore, additional stress-free silicon parameters are required to more fully populate Chandrasekhar's data[24]. Raman spectra of the globules mentioned previously were acquired for both an as-received plate and a heat-treated plate. The heat treatment was performed at 1300°C for one hour in a carbon furnace under an argon atmosphere. The mean wavenumbers decreased considerably from the as-received to the heat-treated plate, from $508.92\ cm^{-1}$ to $506.42\ cm^{-1}$. The asymmetry parameter, q, also decreased (became more asymmetric), and the peak half width value increased. These behaviors indicate an increase in the boron activation level[24]. Both the as-received and heat-treated values indicate higher activated boron levels than those found in literature (although the actual dopant concentration is unknown). Therefore, the parameters determined from these fits can be utilized in extending the Chandrasekhar parameters into higher boron activation concentrations than those found in literature. Figure 4 illustrates the extreme asymmetry found in the heat-treated panel globules. This

particular point has a Fano wavenumber of $506.39\,cm^{-1}$, a half-width of $12.96\,cm^{-1}$, and an asymmetry parameter of 1.84. The closed circle data points are from the experimental measurement, the bold "Profile Fit" line is the overall summation of the fit, the various broken lines are the components of the overall fit, and the open circles are the residuals between the experimental data and the curve fit. It should be noted the Fano effect on most silicon profiles was not this extreme, but exhibited more subdued Fano characteristics and could often be mistaken for a Lorentzian curve.

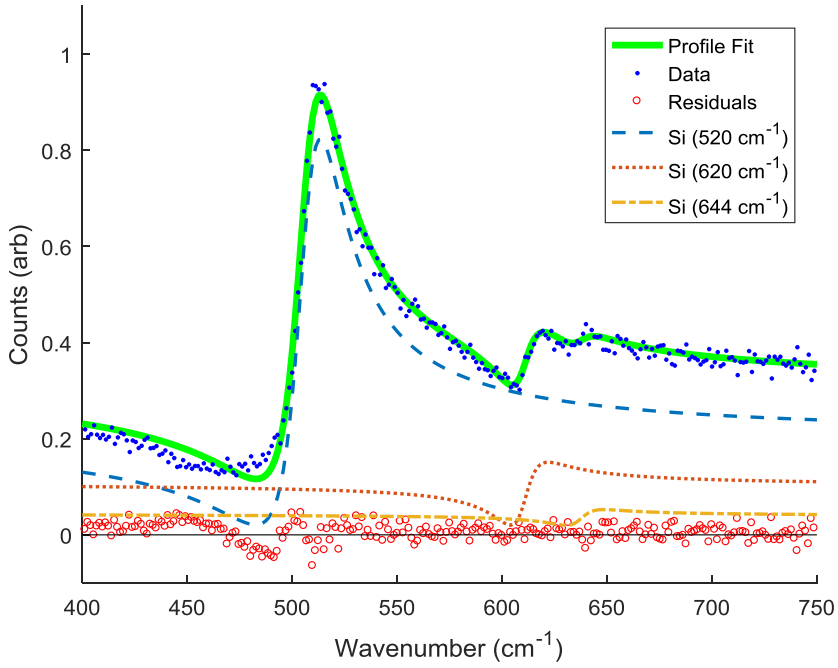

Figure 4: Plot of Raman spectra as a function of wavenumber for an individual silicon globule after heat treatment found on the outer face of a CMC plate. This profile exhibits very high asymmetry, very large peak width, and a peak at $509.91\,cm^{-1}$, which is shifted considerably from undoped and unstressed silicon. The characteristic Fano wavenumber is shifted further still, to approximately

$506.39\ cm^{-1}$. Two additional peaks are seen around $620\ cm^{-1}$ and $644\ cm^{-1}$, which correspond to the boron isotopes ^{11}B and ^{10}B, respectively.

Figure 5 plots the Fano wavenumber versus half-width for the as-received (AR, open circles) and heat treated (HT, open squares) globules. Values from

Table 1 are also plotted, with linear interpolations in-between the values. Finally, a least-squares fit was performed on the current dataset to build an extension for higher levels of dopant, fixing the fitted line to the highest-doped Chandrasekhar data point[24]. Although the dopant level is unknown, large dopant gradients are found throughout the silicon matrix, and this line can be used for stress estimation in further analyses. A similar exercise was performed to determine an appropriate asymmetry value at high dopant levels for a $514.5\ nm$ laser wavelength. The extended values determined from these analyses, along with tabulated Chandrasekhar values for a $514.5\ nm$ laser, are given in

Table 1.

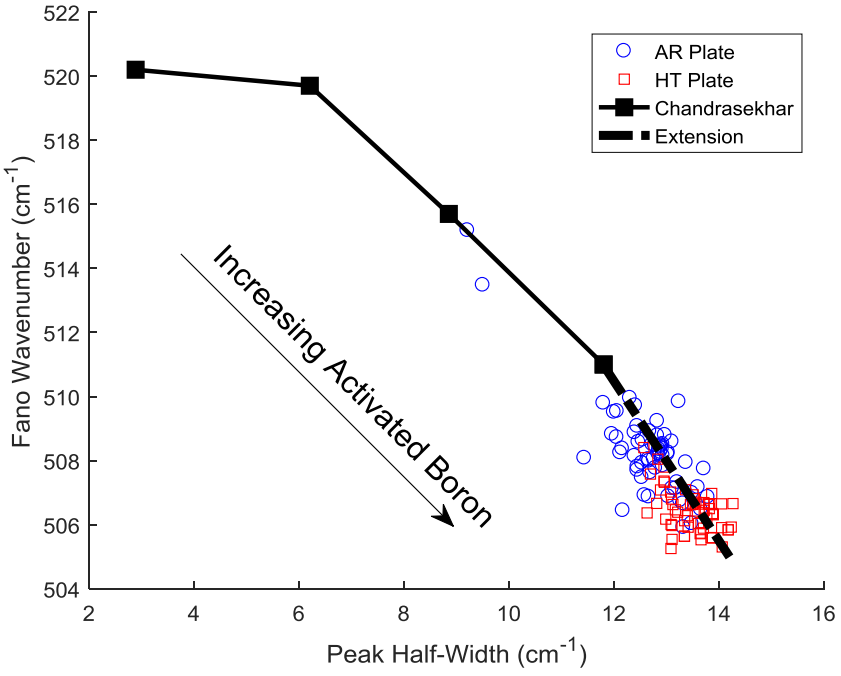

Figure 5: Plot of the stress-free wavenumber versus peak half-width values developed by Chandrasekhar[24], illustrating the measurements taken to build an extension to these data. The circles and squares represent stress-free measurements taken from silicon globules from a CMC plate that was in the as-received and heat treated conditions, respectively. A best-fit extension was produced using a least-squares fitting routine. Increasing peak half width and decreasing wavenumbers are indicative of increasing activated boron in silicon.

Table 1: Tabulated Fano parameters of boron-doped silicon[24], extended with this work.

Dopant Concentration ($atoms/cm^3$)	Asymmetry Parameter (q)	Width Parameter (Γ, cm^{-1})	Fano Wavenumber (ω_0, cm^{-1})
1.5×10^{19}	N/A[1]	2.88	520.2
6×10^{19}	N/A[1]	6.2	519.7
1.5×10^{20}	N/A[1]	8.85	515.7
4×10^{20}	2.57	11.8	511
N/A[2]	1.70	14.20	505

[1]Asymmetry parameters are missing for the lowest concentrations as the Chandrasekhar values were not obtained with a $514.5\ nm$ laser.

[2]The highest dopant concentration is unknown (determined through this work).

The amount of Fano resonance between the three areas investigated (silicon beneath silicon carbide particles, silicon on the surface of the material, and silicon in between fibers within a transverse fiber tow) all exhibited Fano profiles, with consistent trends between each particular area. The silicon found beneath silicon carbide particles was found to have the least amount of activated boron, and thus the Raman signature had the least asymmetry, smallest half-width, and least deviation from the pure silicon stress-free characteristic Raman wavenumber of $520.5\ cm^{-1}$, shown

as open circles in Figure 6. The silicon found directly in the center of various fibers showed the greatest amount of activated boron, having the largest half-widths, and also the largest deviation from pure silicon, shown as open triangles in Figure 6. Finally, the surface silicon displayed varying amounts of activated boron, as indicated by the very large range of wavenumbers and half-width values, and are shown as open squares in Figure 6. When plotted as characteristic wavenumber versus half-width, along with the extended Chandrasekhar values, the Fano wavenumbers were found to follow the Chandrasekhar/experimentally extended stress-free curve and were nearly always slightly above this stress-free line, an indication that the silicon is under a compressive state of stress.

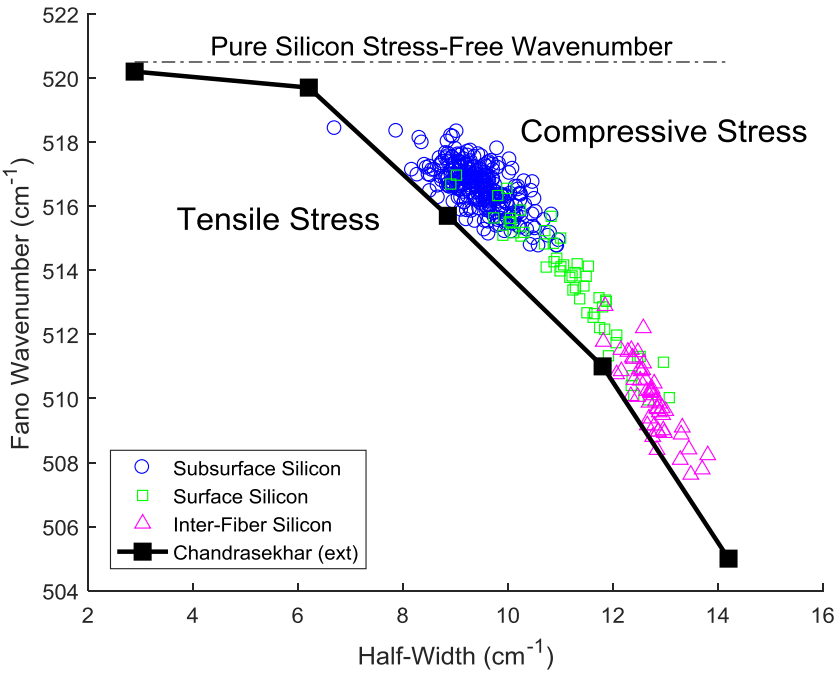

Figure 6: Various as-received silicon wave numbers vs half-width parameters are shown. Large gradients of activated boron are found throughout the various microstructural CMC matrix areas. Without accounting for the activated boron, the upper “Pure Silicon Stress-Free Wavenumber”

dotted line would be utilized to determine if stresses were compressive (above the line) or tensile (below the line). By utilizing the Fano half-width parameter, stressed measurements found below the bold extended Chandrasekhar curve are in a tensile stress state, while stressed measurements above the curve are in a compressive state.

The general methodology developed by Anastassakis[13, 14] to determine the residual stress state relies solely on the difference between the stress-free reference and the stressed material. Obviously, this methodology results in critical errors for doped silicon stress determination. By determining the difference between a stress-free interpolated line and each data point, an accurate stress reading can be produced. In this way, the current methodology extends that of Anastassakis by determining the stress free wavenumber as a function of peak half-width to account for active boron.

Utilizing the stress-free lines in the wavenumber versus half-width plot above, the following methodology is applied to every measurement:

1) The fitting routine outputs the characteristic Fano wavenumber, the half-width parameter, and the asymmetry parameter for each Raman spectra recorded.
2) The stress-free wavenumber at this half-width is determined through linear interpolation of the respective stress-free lines.
3) The difference in wavenumber between the stress-free wavenumber and the wavenumber of the measured point is determined.

4) The wavenumber difference is converted to a stress value through the standard Anastassakis wavenumber to hydrostatic stress relationship, as found in Equation 1.

3.2 Central Intratow Silicon Stress

Scans were collected directly on the center of the silicon found in-between fibers. These points displayed very high asymmetry of the Fano profile, indicating very high levels of activated boron within these areas. Sixty single-point intratow measurements are shown as open triangles in Figure 6. Utilizing the methodology from above, the as-received hydrostatic stress is found to be in compression, with a mean of $-240\ MPa$ and a standard deviation of $100\ MPa$. The mean standard error is $0.13\ cm^{-1}$, which corresponds to $20\ MPa$ (using Equation 1). The standard error incorporates both the Anastassakis[13] uncertainty value ($\pm 0.05\ cm^{-1}$) and the uncertainty due to the numerical fitting routine[32].

3.3 Subsurface Silicon Stress

Sub-surface silicon measurements are shown to exhibit the least amount of activated boron, as evidenced by the relatively low Fano half-width of the silicon profiles open circles in Figure 6. This is due to a combination of the high laser absorption found in silicon (the laser interrogates only a few hundred nanometers into the silicon) as well as boron-depletion in silicon near SiC grain boundaries. When the laser light travels through the silicon carbide particle, the first silicon the light encounters touches the SiC particle grain. These silicon areas consistently show depletion of activated boron.

The depletion zones represent either a lack of boron atoms entirely or a lack of electrically-active boron atoms, with Raman spectroscopy being unable to distinguish between these two cases.

The mean hydrostatic stress in subsurface silicon is found to be $330\ MPa$ in compression. This is due to the higher CTE of silicon carbide than that of silicon, which produces an overall compressive state of stress in the silicon while a tensile stress state is found in the SiC to equilibrate the stress levels[33, 34, 35]. The standard deviation of these stresses is $120\ MPa$. The mean standard error due to fitting is $0.085\ cm^{-1}$, which corresponds to $15\ MPa$.

The silicon carbide Raman signatures were analyzed by fitting three peaks to the α-SiC peaks around $767\ cm^{-1}$, $789\ cm^{-1}$, and $797\ cm^{-1}$. The most intense peak (at $789\ cm^{-1}$) was utilized to determine the residual stress state using the normal methodologies[15]. The silicon carbide particles were determined to exhibit an average hydrostatic residual tensile stress of approximately $300\ MPa$ with a standard deviation of approximately $240\ MPa$.

3.4 Silicon Found on the Surface of the Matrix

An additional silicon area investigated by Raman spectroscopy is the silicon found in-between silicon carbide particles in the overall matrix. These areas are found to exhibit very large gradients of activated boron, as shown through the variation in half-width parameter seen in the open squares in Figure 6. This figure illustrates the large activated dopant distributions generated through the manufacturing process of this material. A standard error of $0.085\ cm^{-1}$, corresponding to $15\ MPa$, was determined from the fitting statistics. Measurements were often taken relatively far from silicon carbide grain boundaries, and thus boron-depleted zones are less common in these measurements.

The mean hydrostatic stress is $320\ MPa$ in compression with a standard deviation of $100\ MPa$, similar to that of the subsurface silicon measurements.

3.5 Silicon Found Throughout Intratow Region

A single area scan of an intratow region was taken to observe stress gradients within the silicon. A representative area is found in Figure 3, where the light-colored center is silicon, the outer dark region is the fiber/Chemical Vapor Infiltrated (CVI) SiC area, and the intersections of the light lines represent the locations of each measurement. Analysis of this area showed significant gradients of activated boron within these regions, with boron depletion evident near the CVI SiC, similar to the boron depletion found behind the SiC particles mentioned previously. This is either a product of a boron segregation/boundary layer effect during melt infiltration or due to boron becoming trapped in an electrically-inactive state near the grain boundaries[26, 36, 37]. In the case of boron segregation, boron atoms would physically not be in the silicon lattice in these areas, likely being robbed by small silicon boride precipitates. In the case of boron entrapment, boron atoms would be present but would not be electrically-active. The two cases are indistinguishable with Raman spectroscopy.

Figure 7 subdues (shown as open squares) the previously graphed data points for the subsurface and surface silicon, and the stress-free line is shown connecting the square

Table 1 values. The intratow region Fano wavenumbers versus half-widths are shown as open circles. Note that these data were not shown in previous figures. The central intratow values previously determined are shown as open triangles as comparison. The central values in the area scan were similar to the central values found earlier, while there are obvious large gradients in the activated boron concentration.

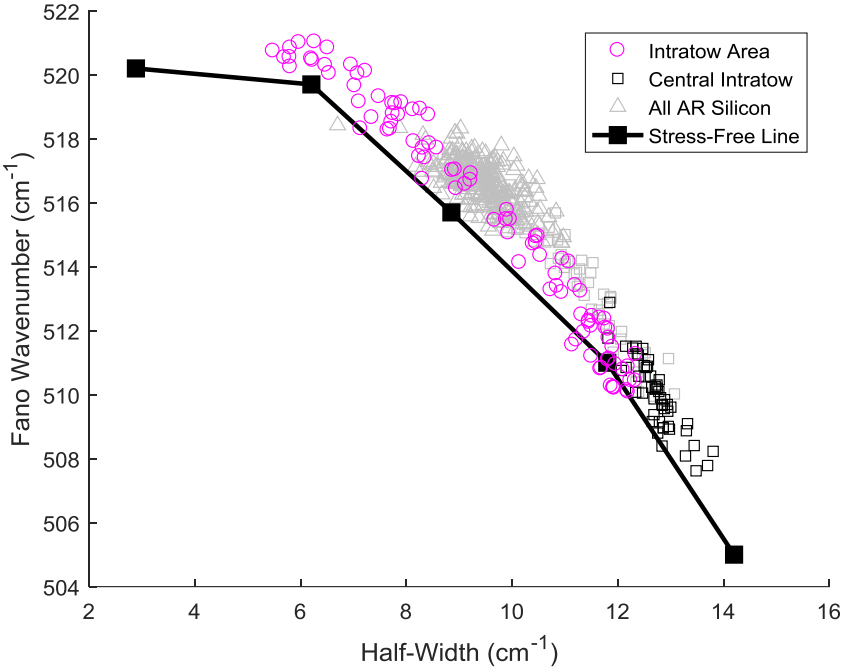

Figure 7: The central portion of each intratow region had very high levels of boron activation, as shown by the triangles above. However, when measurements were taken throughout an entire intratow area, large gradients of boron were found to exist, as indicated by the circles covering a large range of Fano wavenumbers and half-widths. The remaining as-received silicon data are shown by the squares as reference.

Figure 8 displays the map of Fano wavenumbers in the interrogated intratow area shown in Figure 3. The wavenumbers are functions of the boron activation level, and thus are lowered considerably as the activated boron increases near the center of the silicon vein. This phenomenon

of lowered wavenumbers near grain boundaries mimics the behavior of results from Jannotti, et al.[38]; however, Jannotti did not take the half-width or asymmetry of the reported Fano profiles into account, and reported large tensile stresses in these areas that are likely to have been an erroneous interpretation of the data. Figure 9 displays the half-width of the Fano profiles per the investigated points of the area scan, which qualitatively illustrates the boron activation levels of the various points. Finally, Figure 10 illustrates the corrected stress distribution within the intratow area under investigation.

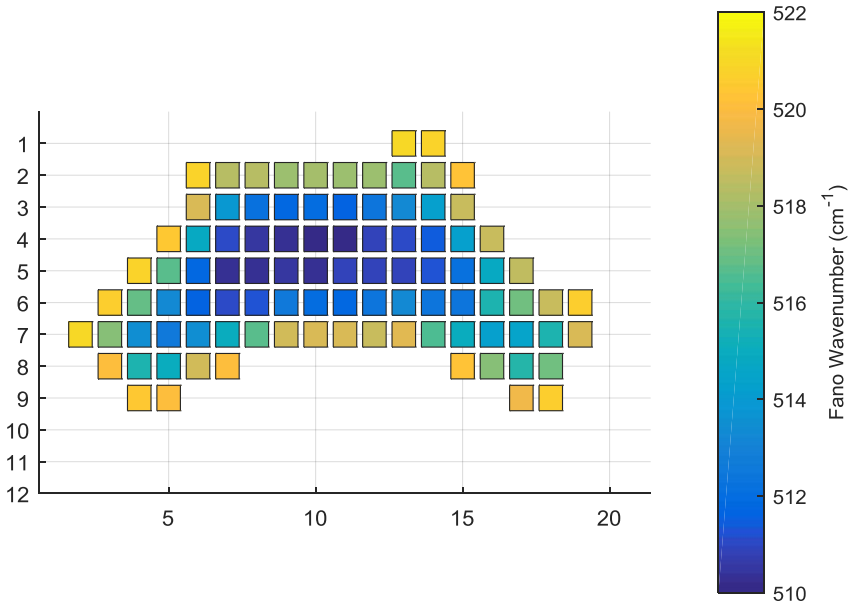

Figure 8: Fano wavenumber results of intratow area scan shown in Figure 3 at room temperature. Very low wavenumbers in the center are indicative of either high tensile stresses or high

concentrations of activated boron. Additional parameters from the Raman spectra are required to determine the stress state. Measurements taken in $1\ \mu m$ intervals.

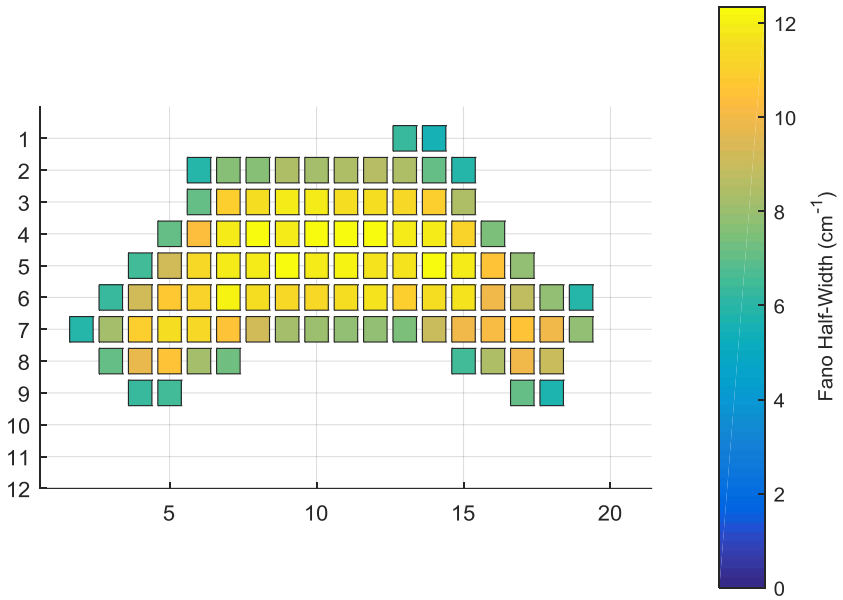

Figure 9: Fano half-width parameter results of intratow area scan shown in Figure 3 at room temperature (determined from the same scan data as Figure 8). The large peak widths, especially near the center, is indicative of high concentrations of boron dopant within the silicon.

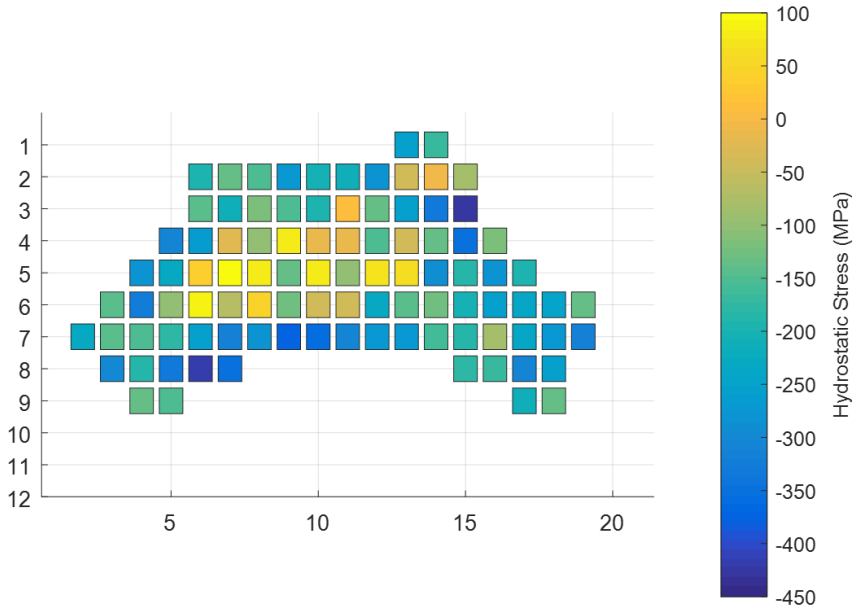

Figure 10: The Fano wavenumber and half-width must be utilized collectively to determine the stress state at each measurement point, as shown in the figure above. Hydrostatic stresses in this sample between 425 MPa in compression to 90 MPa in tension.

Hydrostatic stresses ranged from $425\ MPa$ in compression to $90\ MPa$ in tension, with an average value of $180\ MPa$ in compression and a standard deviation of $120\ MPa$. Large stress variations are expected due to the small laser spot size investigating local stress values[17]. Hi-Nicalon fibers have a lower CTE than silicon[39, 40], and thus the proximity of this investigated silicon to the fibers is likely affecting this stress state to be in overall less compression than other silicon found throughout the composite. However, very large incorrect tensile stresses (up to ~2 GPa) would have been calculated had the Fano parameters not been taken into account. Stresses in the silicon matrix phase and silicon carbide (when applicable) are summarized in Table 2 for all cases studied.

Table 2: Summary of silicon and silicon carbide hydrostatic stresses

Measured area	Mean silicon hydrostatic compressive stress	Mean silicon carbide hydrostatic tensile stress
Central intratow	240 MPa	-
SiC particle/ subsurface silicon	330 MPa	300 MPa
Surface silicon	320 MPa	-
Intratow general area	170 MPa	-

4.0 Conclusions

Activated boron concentration levels must be incorporated into stress determinations to accurately describe the decreased silicon wavenumbers found in doped silicon. Without incorporation of these effects, the stresses determined through Raman spectroscopy will be more tensile than reality and will lead to exceptionally large standard deviations of stress. Additionally, activated boron is found to be depleted near silicon carbide grain boundaries due to grain boundary segregation or electrical inactivation. Silicon stresses in-between fibers within fiber tows exhibited considerably less compressive stress than the silicon stresses found in the general matrix areas due to the low CTE values of Hi-Nicalon fibers versus silicon. The mean intratow silicon stress throughout the entire intratow silicon vein area is approximately $180\ MPa$ in compression, while the silicon mean compressive hydrostatic stresses in the general matrix areas are approximately $300\ MPa$.

Funding and Competing Financial Interests

Research funding provided by US Air Force; materials provided by Rolls Royce.

Ownership

The authors declare that the submitted work is our own and that copyright has not been breached in seeking publication.

Originality

The authors declare that the submitted work has not previously been published in full, and is not being considered for publication elsewhere. A partial presentation of this material was presented at the United States Advanced Ceramics Association January 2018 conference in Cape Canaveral, FL

References

[1]Ohnabe H, Masaki S, Onozuka M, et al. Potential application of ceramic matrix composites to aero-engine components. *Composites Part A.* 1999;30(4):489-496.

[2]Singh Y, Mansour R, Morscher G. Combined acoustic emission and multiple lead potential drop measurements in detailed examination of crack initiation and growth during interlaminar testing of ceramic matrix composites. *Composites Part A.,* 2017;97:93-99.

[3]Choi D, Shinavski RJ, Steffier WS, et al. Residual stress in thick low-pressure chemical-vapor deposited polycrystalline SiC coatings on Si substrates. *J. Appl. Phys.* 2005;97(7):074904.

[4]Wing BL, Halloran JW. Microstress in the matrix of a melt-infiltrated SiC/SiC ceramic matrix composite. *J. Am. Ceram. Soc.* 2017;100(11):5286-5294.

[5]Wing B, Esmonde-White F, Halloran J. Microstress in reaction-bonded SiC from crystallization expansion of silicon. *J. Am. Ceram. Soc.* 2016;99(11):3705-3711.

[6]Bobet J, Lamon J. Study of thermal residual stresses in ceramic matrix composites. *J. Alloys Compd.* 1997;259:260-264.

[7]Ramìrez-Rico J, Stolzenburg F, Almer J, et al. In situ imaging and strain determination during fracture in a SiC/SiC ceramic matrix composite. *Scripta Mater.* 2013;69(7):497-500.

[8]Harder B, Almer J, Weyant C, et al. Residual stress analysis of multilayer environmental barrier coatings. *J. Am. Ceram. Soc.* 2009;92(2):452-459.

[9]Morscher G, Gordon N. Acoustic emission and electrical resistance in SiC-based laminate ceramic composites tested under tensile loading. *J. Eur. Ceram. Soc.* 2017;37(13):3861-3872.

[10]Mei H. Measurement and Calculation of Thermal Residual Stress in Fiber Reinforced Ceramic Matrix Composites. *Compos. Sci. Technol.* 2008;68(15):3285-3292.

[11]De Wolf I. Micro-Raman spectroscopy to study local mechanical stress in silicon integrated circuits. *Semicond. Sci. Technol.* 1996;11(2):139-154.

[12]Anastassakis E, Pinczuk A, Burstein E. Effect of static uniaxial stress on the Raman spectrum of silicon. *Solid State Commun.* 1969;8(2):133-138.

[13]Anastassakis E, Cantarero A, Cardona M. Piezo-Raman measurements and anharmonic parameters in silicon and diamond. *Phys. Rev. B: Condens. Matter.* 1990;41(11):7529-7535.

[14]Anastassakis E. Strain characterization of polycrystalline diamond and silicon systems. *J. Appl. Phys.* 1999;86(1):249-258.

[15]DiGregorio J, Furtak T. Analysis of Residual Stress in 6H-SiC Particles within Al2O3/SiC Composites through Raman Spectroscopy. *J. Am. Ceram. Soc.* 1992;75(7):1854-1857.

[16]Gouadec G, Colomban P, Bansal NP. Raman Study of Hi-Nicalon Fiber Reinforced Celsian Composites: II, Residual Stress in Fibers. *J. Am. Ceram. Soc.* 2001;84(5):1136-1142.

[17]Withers P, Bhadeshia H. Residual stress, Part 1 - Measurement techniques. *J. Mater. Sci. Technol.* 2001;17:355-364.

[18]Brown M, Arnold C. Fundamentals of laser-material interaction and application to multiscale surface modification. In *Laser precision microfabrication*, Springer Berlin Heidelberg; 2010:91-120.

[19]Aspnes D, Studna A. Dielectric functions and optical parameters of Si, Ge, GaP, GaAs, GaSb, InP, InAs, and InSb from 1.5 to 6.0 eV. *Phys. Rev. B: Condens. Matter.* 1983;27(2):985-1009.

[20]Derst G, Wilbertz C, Bhatia K, et al. Optical properties of SiC for crystalline/amorphous pattern fabrication. *Appl. Phys. Lett.* 1989;54(18):1722-1724.

[21]Suyama S, Kameda T, Itoh Y. Effect of structure of interfacial coating layer on mechanical properties of continuous fiber reinforced reaction sintered silicon carbide matrix composite. *J. Mater. Sci.* 2002;37(6):1101-1106.

[22]Fano U. Effects of configuration interaction on intensities and phase shifts. *Physical Review.* 1961;124(6):1866-1878.

[23]Cerdeira F, Fjeldly R, Cardona M. Raman study of the interaction between localized vibrations and electronic excitations in boron-doped silicon. *Physical Review B.* 1974;9(10):4344-4350.

[24]M. Chandrasekhar, H. R. Chandrasekhar, M. Grimsditch and M. Cardona, "Study of the localized vibrations of boron in heavily doped Si. *Phys. Rev. B: Condens. Matter.* 1980;22(10):4825-4833.

[25]Nickel N, Lengsfeld P, Sieber I. Raman spectroscopy of heavily doped polycrystalline silicon thin films," *Phys. Rev. B: Condens. Matter.* 2000;61(23):558-561.

[26]Pichler P. Intrinsic Point Defects. In Intrinsic Point Defects, Impurities, and Their Diffusion in Silicon. Springer, Vienna. 2004:77-227.

[27]Agaiby RMB, Becker M, Thapa SB, et al. Stress and doping uniformity of laser crystallized amorphous silicon in thin film silicon solar cells. *J. Appl. Phys.* 2010;107(5):054312.

[28]Cerofolini GF, Meda L. Physical Chemistry of, in and on Silicon. Springer Science & Business Media; 2012.

[29]Fahey P, Griffin P, Plummer J. Point defects and dopant diffusion in silicon. *Reviews of Modern Physics.* 1983;61(2):289-388.

[30]Aboy M, Pelax L, Barbolla J, et al. Boron activation and redistribution during thermal treatments after solid phase epitaxial regrowth. *Mater. Sci. Eng., B*. 2005;124:205-209.

[31]Sadigh B, Lenosky T, Caturla M, et. Al. Large enhancement of boron solubility in silicon due to biaxial stress. *Appl. Phys. Lett.* 2002;80(25):4738-4740.

[32]Montgomery, D. Design and Analysis of Experiments, 6th ed., John Wiley & Sons, Inc., 2004.

[33]Okada Y, Tokumaru Y. Precise Determination of Lattice Parameter and Thermal Expansion Coefficient of Silicon Between 300 and 1500K. *J. Appl. Phys.* 1984;56(2):314-320.

[34]Li Z, Bradt R. Thermal expansion of the hexagonal (6H) polytype of silicon carbide. *J. Am. Ceram. Soc.* 1986;69(12):863-866.

[35]Inoue Z, Kurachi Y. Structure change of SiC at high temperature. Proceedings of the International Symposium on Ceramic Components for Engines; 1983; Tokyo.

[36]Sim B, Kim K, Lee H. Boron segregation control in silicon crystal ingots grown in Czochralski process. *J. Cryst. Growth.* 2006;290(2):665-669.

[37]Burton J, Prim R, Slichter W. The distribution of solute in crystals grown from the melt. Part I. Theoretical. *J. Chem. Phys.* 1953;21(11):1987-1991.

[38]Jannotti P, Subhash G, Zheng J, et al. Measurement of microscale residual stresses in multi-phase ceramic composites using Raman spectroscopy. *Acta Mater.* 2017;129:482-491.

[39]Katoh Y, Ozawa K, Shih C, et al. Continuous SiC fiber, CVI SiC matrix composites for nuclear applications: Properties and irradiation effects. *J. Nucl. Mater.* 2014;448(1):448-476.

[40]Corman G, Luthra K, Jonkowski J, et al. Melt infiltrated ceramic matrix composites for shrouds and combustor liners of advanced industrial gas turbines. General Electric Company; 2011.